Quasi-phase matched second-harmonic generation through thermal poling in femtosecond laser-written glass waveguides

Guangyu Li[1], Kim A. Winick[2*], Ali A. Said[3], Mark Dugan[3], and Philippe Bado[3]

[1]*Currently with Electro-Scientific, 13900 NW Science Park Drive, Portland, OR 97229, USA*
[2]*Department of Electrical Engineering and Computer Science, University of Michigan, Ann Arbor, MI 48109, USA*
[3]*Translume, Inc. 655 Phoenix Drive, Ann Arbor, MI 48108, USA*
**Corresponding author: winick@eecs.umich.edu*

Abstract: Quasi-phase matched second-harmonic generation at 532 nm is demonstrated in a channel waveguide that is written in bulk fused silica using a femtosecond laser. The second-order nonlinear grating is fabricated using uniform thermal poling followed by periodic erasure inside an e-beam deposition system caused, by what we believe to be, x-rays. A SHG conversion efficiency of 2×10^{-5} %/W-cm^2 was obtained for a 1 cm long device, corresponding to an effective nonlinear coefficient of 0.0075 pm/V.

©2009 Optical Society of America

OCIS codes: (130.0130) Integrated optics; (190.2620) Frequency conversion; (190.4400) Nonlinear optics, materials; (190.4360) Nonlinear optics, devices.

References and links

1. R. A. Myers, N. Mukherjee, and S. R. J. Brueck, "Large second-order nonlinearity in poled fused silica," Opt. Lett. **16,** 1732–1734 (1991).
2. A. C. Liu, J. F. Digonnet, and G. S. Kino, "Electro-optic phase modulation in a silica channel waveguide," Opt. Lett. **19**, 466-468 (1994).
3. O. Tarasenko and W. Margulis, "Electro-optic fiber modulation in a Sagnac inteferometer," Opt. Lett. **32**, 1356-1358 (2007).
4. V. Pruneri and P. G. Kazansky, "Frequency doubling of picosecond pulses in periodically poled D-shape silica fiber," Electron. Lett. **33**, 318–319, (1997).
5. H.-Y. Chen, J.-S. Sue, Y.-H. Lin, and S. Chao, "Quasi-phase-matched second-harmonic generation in ultraviolet-assisted periodically poled planar fused silica," Opt. Lett. **28**, 917–919 (2003).
6. P. G. Kazansky, L. Dong, and P. S. J. Russell, "Vacuum poling: an improved technique for effective thermal poling of silica glass and germanosilicate optical fibers," Electron. Lett. **30**, 1345–1346 (1994).
7. P. G. Kazansky, A. Kamal, and P. S. J. Russell, "Erasure of thermally poled second-order nonlinearity in fused silica by electron implantation," Opt. Lett. **18**, 1141–1143 (1993).
8. J. M. Dell, M. J. Joyce, and G. O. Stone, "Erasure of poling-induced second-order optical nonlinearities in silica by uv exposure," in Proceedings of SPIE **2289**, 185–193 (1994).
9. S. Montant, A. L. Calvez, E. Freysz, A. Ducasse, V. Nazabal, E. Fargin, and G. L. Flem, "Light-controlled erasure of induced $\chi^{(2)}$ in thermally poled glass," Appl. Phys. Lett. **74**, 2623–2625 (1999).
10. H.-Y. Chen, J.-S. Sue, Y.-H. Lin, and S. Chao, "Quasi-phase-matched second-harmonic generation in ultraviolet-assisted periodically poled planar fused silica," Opt. Lett. **28**, 917–919 (2003).
11. H.-Y. Chen, C.-L. Lin, Y.-H. Yang, S. Chao, H. Niu, and C. T. Shih, "Creation of second-order nonlinearity and quasi-phase- matched second-harmonic generation in Ge-implanted fused silica planar waveguide," Appl. Phys. Lett. **86**, 081107 (2005).
12. S. Chao, H.-Y. Chen, Y.-H. Yang, Z.-W. Wang, C. T. Shih, and H. Niu, "Quasi-phase-matched second-harmonic generation in Ge-ion implanted fused silica channel waveguide," Opt. Express **13**, 7091–7096 (2005).
13. J. Fage-Pedersen, R. Jacobsen, and M. Kristensen, "Planar glass devices for efficient periodic poling," Opt. Express **13**, 8514–8519 (2005).
14. R. Schineller, R. P. Flam and D. W. Wilmot, "Optical waveguides formed by proton irradiation of fused silica," J. Opt. Soc. Am. **58**, 1171-1176 (1968).
15. J. Bell and C. N. Ironside, "Channel optical waveguides directly written in glass with an electron beam," Electron. Lett. **27**, 448-450 (1991).
16. K. Miura, J. Qiu, H, Inouye, and T. Mitsuyu, "Photowritten optical waveguides in various glasses with ultrashort laser pulses," Appl. Phys. Lett. **71**, 3329-3331 (1997).

#109008 - $15.00 USD Received 23 Mar 2009; revised 12 May 2009; accepted 15 May 2009; published 21 May 2009

17. C. Florea and K. A. Winick, “Fabrication and characterization of photonic devices directly-written in glass using femtosecond laser pulses,” J. Lightwave Technol. **21**, 246-253 (2003).
18. A. M. Kowalevicz, V. Sharma, E. P. Ippen, J. G. Fujimoto, and K. Minoshima, “Three dimensional photonic devices fabricated in glass by use of a femotosecond laser oscillator, Opt. Lett. **30**, 1060-1062 (2005).
19. G. Li, K. A. Winick, A. A. Said, M. Dugan, and P. Bado, “A waveguide electro-optic modulator in fused silica fabricated by femtosecond laser direct writing and thermal poling,” Opt. Lett. **31**,739-741 (2006).
20. Gaungyu Li, K. A. Winick, Ali Said, Mark Dugan and Phillipe Bado, "Nonlinear Optical Waveguide Devices Based on Femtosecond Laser Direct Writing and Thermal Poling in Fused Silica," *OSA Frontiers in Optics Annual Meeting*,Tucson, Arizona, October 16-20 (2005), post-deadline paper PDP-B7.
21. F. P. Mezzapesa, I. C. S. Carvalho, C. Cortari, P. G. Kazansky, J. S. Wilkinson, and G. Chen, “Voltage-assisted cooling: a new route to enhance $\chi^{(2)}$during thermal poling,” in *Conference on Lasers and Electro-Optics*, Technical Digest (Optical Society of America 2005), paper CMW7.
22. H. An and S. Fleming, “Visualization of second-order nonlinear layer in thermally poled fused silica glass,” Appl. Phys. Lett. **85**, 5819–5821 (2004).
23. W. Margulis and F. Laurell, “Interferometric study of poled glass under etching,” Opt. Lett. **21**, 1786–1788, 1996.
24. R. Blum, A. Truhins, B. Poumellec and S. Zhao, “The use of X-ray-induced and thermostimulated visible and UV luminescence for understanding X-ray poling of silica glasses,” J. of Luminescence **122-123**, 137-141 (2007).
25. L. Gerward, “X-ray attenuation coefficients and atomic photoelectric absorption cross sections of silicon,” J. At. Mol. Phys. **14**, 3389-3395 (1981).
26. R. H. Millar and J. R. Greening, “Experimental x ray mass attenuation coefficients for materials of low atomic number in the energy range 4 to 25 keV,” J. At. Mol. Phys. **7**, 2332-2344 (1974).
27. T. E. Everhart an P. H. Hoff, “Determination of kilovolt electron energy dissipation vs penetration distance in solid materials,” J. Appl. Phys. **42**, 5837-5846 (1971).
28. A. Yariv,*Optical Electronics in Modern Communications*, 5th Ed. (Oxford 1997), Chap. 8.
29. T. Toyoda and M. Yabe, “The temperature dependence of the refractive indices of fused silica and crystal quartz,” J. Appl. Phys. **16**, L97– L100 (1983).
30. J. M. Jewell, “Thermooptic coefficients of some standard reference material glasses,” J. Am. Ceram. Soc. **74**, 1689–1691 (1991).
31. H. An, S. Fleming, B. W. McMillen, K. P. Chen, and D. Snoke, “Thermal poling induced second-order nonlinearity in femtosecond laser-modified fused silica,” Appl. Phys. Lett. **93**, 061115-1 – 061115-3 (2008).
32. J. Beermann, S. Bozhevolnyi, K. Pedersen, J. Fage-Pedersen, “High-resolution second harmonic microscopy of poled silica waveguides,” Opt. Comm. **221**, 295-300 (2003).
33. C. Corbari, J. D. Mills, O. Deparis, B. G. Klappauf, and P. G. Kazansky, “Thermal poling of glass modified by femtosecond laser irradiation,” Appl. Phys. Lett. **81**, 1585–1587 (2002).

1. Introduction

Silica based planar optical devices are of great importance in optical communication systems because silica glass has excellent transparency from the UV to the near-IR, good chemical/structural durability and is fiber compatible. Glass, however, is an amorphous material with effective inversion symmetry. This symmetry precludes both electro-optic (EO) light control and wavelength conversion in glass by second-order, nonlinear, parametric processes, and thus limits the functional utility of glass integrated optical devices.

In 1991 Myers et al. demonstrated that thermal poling could be used to induce a second order susceptibility, $\chi^{(2)}$, on the order of 1 pm/V in fused silica [1]. The thermal poling technique has been utilized to realize both EO modulation [2, 3] and quasi-phase matched (QPM) second harmonic generation (SHG) in silica fibers and planar, glass substrates [4, 5]. QPM $\chi^{(2)}$ grating structures can be fabricated by periodic poling with patterned periodic electrodes [6] or by selective erasure of uniformly poled regions [7-9]. Selective erasure has been achieved using focused electron beams [7], ultraviolet exposure [8] and two-photon absorption of near-IR laser radiation [9]. Chen et al. reported QPM-SHG in a planar bulk piece of fused silica achieved by periodic UV-erasure of uniformly poled regions [10]. Chen et al. subsequently extended these results to both planar and channel waveguide QPM-SHG devices fabricated in fused silica by Ge-implantation [11,12]. The normalized conversion efficiency for the 7 mm long channel waveguide device reported in [12] was 6.1×10^{-4} %/W/cm^2, corresponding to an effective nonlinear coefficient, d_{eff}, of 0.005 pm/V. More recently, a thin-film, SHG, glass, waveguide device, based on silica-on-silicon technology, was demonstrated using thermal poling with embedded periodic electrodes [13]. The device consisted of a buried silicon oxynitride (SiON) waveguide and a 3 mm long QPM $\chi^{(2)}$ grating.

#109008 - $15.00 USDReceived 23 Mar 2009; revised 12 May 2009; accepted 15 May 2009; published 21 May 2009
(C) 2009 OSA

A normalized conversion efficiency of 1.4×10^{-3} %/W/cm^2 was obtained, corresponding to an effective nonlinear coefficient of 0.02 pm/V, which is the highest value reported to date for a thermally poled QPM-SHG device. This value is still more than an order of magnitude below the peak nonlinearity achieved by thermal poling in bulk fused silica. Thus there are potential advantages associated with using bulk fused silica, as opposed to thin films, to fabricate nonlinear parametric waveguide devices. The techniques available to fabricate waveguides in bulk fused silica are limited to ion implantation [12,14], electron beam irradiation [2,15] and femtosecond laser direct writing [16]. As opposed to ion implantation, femtosecond laser direct writing is a mask-less process. The later technique also offers the ability to write waveguides in three dimensions, a functionality that is unachievable using electron beam writing.

In the last six years, femtosecond laser direct writing technology has been developed to the point that low-loss, complex, waveguide devices can be fabricated in fused silica [17,18]. As reported in [19], this technology can be combined with thermal poling to realize EO waveguide devices in bulk fused silica substrates. In this paper, a waveguide QPM-SHG device is fabricated using femtosecond laser direct writing in bulk fused silica for the first time. The QPM structure is realized by uniform thermal poling followed by periodic erasure of the $\chi^{(2)}$. A new technique, which relies on the use of a standard electron-beam (e-beam) deposition system, is used to perform the periodic erasure [20]. A normalized conversion efficiency of 2×10^{-5} %/W/cm^2 was obtained for a 1 cm long device, corresponding to an effective nonlinear coefficient of 0.0075 pm/V.

2. Device fabrication

2.1 Thermal poling of bulk fused silica

A 1.6 mm thick Herasil fused silica sample measuring 45 mm × 25 mm was sandwiched between two pieces of an n-type silicon wafer and thermally poled with an applied voltage of 4 kV inside a box furnace at a temperature of 275 °C. After ten minutes, the furnace was turned off, the applied voltage was increased to 5 kV, and the sample was allowed to cool to room temperature [21]. Upon returning to room temperature, the voltage was turned off and the sample was removed from the oven. A standard Maker fringe measurement was performed on the poled sample, and the result is shown in Fig. 1.

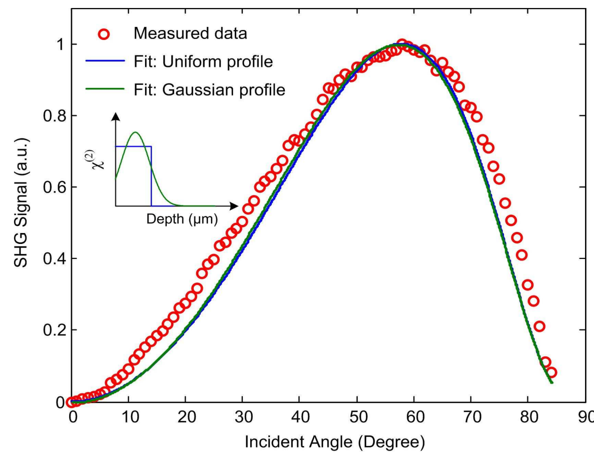

Fig. 1. Maker fringe data from thermally poled fused silica.

This Maker fringe data by itself is not sufficient to reconstruct the spatial profile of the induced nonlinearity, $\chi_{33}^{(2)}$. In order to compare our results with those previously reported, as well as obtain a crude estimate of the thickness of the nonlinear layer, we assumed that the profile was either step-like or Gaussian in shape. As can be seen in Fig. 1, both of these

#109008 - $15.00 USD Received 23 Mar 2009; revised 12 May 2009; accepted 15 May 2009; published 21 May 2009
(C) 2009 OSA

assumed profiles were able to produce a reasonable fit to the measured data, though recent evidence indicates that the Gaussian profile is probably the more accurate representation [22]. The absolute magnitude of the induced $\chi_{33}^{(2)}$ was determined by making a reference Maker fringe measurement on a piece of x-cut crystal quartz with a known d_{11} coefficient of 0.5 pm/V. Assuming a step-like profile for the induced nonlinearity, the magnitude, $\chi_{33}^{(2)}$, and the depth of the nonlinear region were estimated to be 0.25 pm/V and 18 μm, respectively.

2.2 Femtosecond laser direct written waveguide

A femtosecond laser operating at a center wavelength of 790 nm, with a pulse width of 110 fs, a pulse repetition rate of 238 kHz, and a pulse energy of 200 nJ was used to write waveguides in the thermally poled glass sample. A microscope objective with a numerical aperture of 0.55 focused the laser beam slightly below the top surface of the sample while the sample was moved on a computer-controlled translation stage at a scan speed of 100 μm/s. The resulting waveguide refractive index profile, $n_{sub} + \Delta n(x,z)$, was measured using a refractive near-field (RNF) profilometer at 658 nm and is shown in Fig. 2.

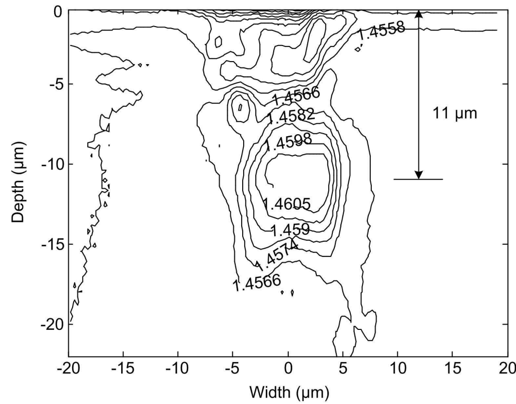

Fig. 2. Measured refractive index profile (at 658 nm) of femtosecond laser written waveguide in fused silica.

The x coordinate axis referred to in this paper is oriented parallel to the sample's surface and perpendicular to the waveguide, while the coordinate z coordinate axis is normal to the surface of the sample.

Using 1.44972 and 1.46081 for the substrate refractive index, n_{sub}, at wavelengths of 1064 nm and 532 nm, respectively (provided by the glass manufacturer), and assuming that the wavelength dispersion of the waveguide index change, Δn(x,z), is negligible (i.e., $n(x,z,\lambda) = n_{sub}(\lambda) + \Delta n(x,z,658\,\text{nm})$, the TE mode profiles, E(x,z), and mode effective indices, N, were numerically computed using the beam propagation method (BPM). The results of these calculations, at both the fundamental (1064 nm) and SHG (532 nm) wavelengths, are shown in Table 1 and Fig. 3 below.

Table 1. Dispersion of fused silica substrate and computed waveguide mode effective indices at 1064nm and 532nm

Refractive Index	1064 nm	532 nm
n_{sub}	1.44972	1.46081
N_{eff}	1.452091	1.464432

#109008 - $15.00 USDReceived 23 Mar 2009; revised 12 May 2009; accepted 15 May 2009; published 21 May 2009
(C) 2009 OSA

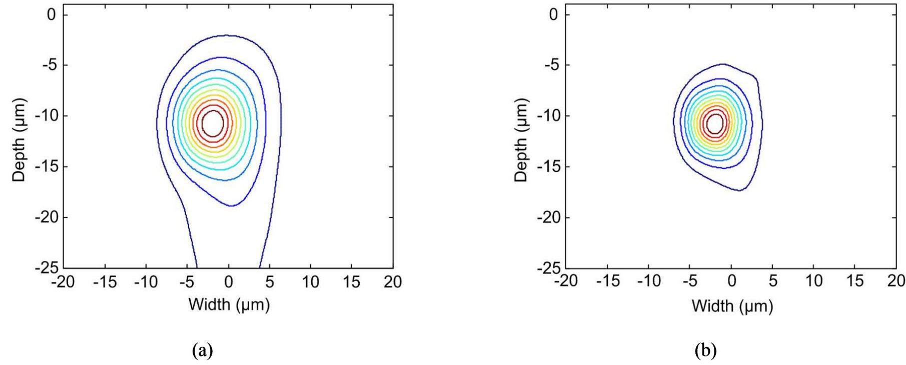

Fig. 3. Computed mode field contour and effective indices at (a) 1064 nm and (b) 532 nm for femotosecond laser-written waveguide in fused silica.

2.3 Design and fabrication of QPM $\chi^{(2)}$ grating

Using the computed mode effective indices at 1064 nm and 532 nm given in Table 1, the required QPM first order grating period was computed from the phase matching condition

$$\Delta k = \frac{2\pi N_{2\omega}}{\lambda_f/2} - 2\frac{2\pi N_{\omega}}{\lambda_f} - \frac{2\pi m}{\Lambda} = 0 \tag{1}$$

to be 43.1 µm, where λ_f and $\lambda_f/2$ are the wavelengths of the fundamental and second-harmonic beams, m is the order of the phase matching, Λ is the grating period, and N_{ω} and $N_{2\omega}$ are the waveguide mode effective indices at the fundamental and second harmonic wavelengths, respectively.

While using an e-beam deposition system to deposit aluminum electrodes on a uniformly poled fused silica sample, it was discovered that the deposition process caused the nonlinearity to be erased. Based on this observation, a new method was developed to fabricate QPM $\chi^{(2)}$ gratings in previously uniformly poled samples [20]. First a silicon grating mask was fabricated. This was accomplished by photolithographically patterning the desired grating in a photoresist layer that had been spun on top of a 200 µm thick silicon wafer. The grating pattern was subsequently transferred entirely through the thickness of the silicon wafer by reactive ion etching using an STS deep silicon etcher. The SEM image of the resulting silicon grating mask is shown in Fig. 4.

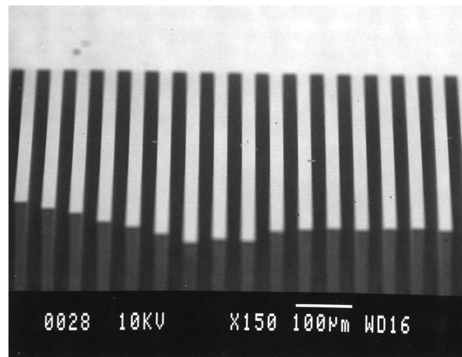

Fig. 4. SEM image of a STS etched silicon grating.

A previously uniformly poled glass sample, containing the femtosecond laser-written waveguide, was spin coated with a layer of photoresist, and then the silicon grating was placed on top of the photoresist layer with the grating groves aligned normal to the underlying

waveguide. The photoresist served as an adhesion layer that could be easily removed at the end of the process. The sample, with the attached silicon grating, was put inside the chamber of an electron-beam deposition system. The deposition parameters were set to a 10 kV beam acceleration, a beam current in the range of 0.2-0.5 A, and a run duration of about 2 minutes. A standard deposition process of 150 nm aluminum was performed. After the run was completed, the glass sample and the silicon mask were separated, and the remaining photoresist was completely removed from the glass.

The etching rate is different for poled and unpoled regions in glass [23]. Thus it was possible to view the periodically erased $\chi^{(2)}$ structure by etching the sample in a 50:50 mixture, by volume, of hydrofluoric acid for 1 minute. The resulting image of the etched glass sample, observed under an optical microscope, is shown in Figure 5. In order to further confirm that selective erasure had occurred, a second, but coarser $\chi^{(2)}$ grating with a period of 400 μm, was fabricated using the above e-beam deposition method in a waveguide-free piece of fused silica. A Q-switched microchip laser operating at 1064 nm was focused to a spot on the surface of this sample, and a transmitted SHG signal was recorded as the spot was scanned across the surface. As shown in Fig. 6, the SHG signal was observed to vary with the same period as the grating. A relatively coarse grating was chosen for these measurements, since it allowed good spatial resolution to be obtained without imposing tight focusing requirements on the fundamental probe beam.

Although the mechanism by which the $\chi^{(2)}$ is erased inside the e-beam evaporator deposition system is not fully understood, the erasure is likely caused by x-ray generation [24] and/or by incident electrons [7] scattered from the target. X-ray (Bremsstrahlung) generation inside the chamber must occur to some degree when the electron beam is stopped by the target, which in this case was aluminum. At 8048 keV (the copper $K\alpha_1$ x-ray line of Al), the x-ray attenuation coefficients in crystalline silicon and SiO_2 are 14.46 mm^{-1} and 8.18 mm^{-1}, respectively and decrease monotonically with increasing x-ray energy [25, 26]. Therefore, a 200 μm thick piece of crystalline silicon will effectively absorb incident x-rays, while the x-rays passing through the openings in the silicon mask will penetrate to a depth of several hundred microns into the poled glass. The penetration depth of 10 keV electrons on the other hand is only a micron or two in both crystalline silicon and SiO_2 [27]. Given this fact, along with the observation that a 10 μm thick film of either photoresist or PMMA deposited on top of the sample did not inhibit erasure of the poled regions of $\chi^{(2)}$, it is suspected that x-rays are responsible, at least in part, for the erasure. This, however, is an area that warrants further study before any definition conclusions may be drawn. Nonetheless, the method described has proven to be a simple technique for fabricating QPM $\chi^{(2)}$ gratings in fused silica.

3. Results and discussion

A 1 cm long waveguide QPM-SHG device was fabricated in bulk fused silica using femtosecond laser direct writing followed by thermal poling and periodic erasure of the poling induced $\chi^{(2)}$. The QPM $\chi^{(2)}$ grating period was chosen to 43.1 μm, which corresponds to first order operation.

3.1 Conversion efficiency

We assume that the poled glass has $C_{\infty v}$ symmetry, with the axis of anisotropy along z direction, and that Kleinman symmetry is satisfied. Thus the nonlinear optic tensor can be described by Eq. (2)

#109008 - $15.00 USDReceived 23 Mar 2009; revised 12 May 2009; accepted 15 May 2009; published 21 May 2009
(C) 2009 OSA

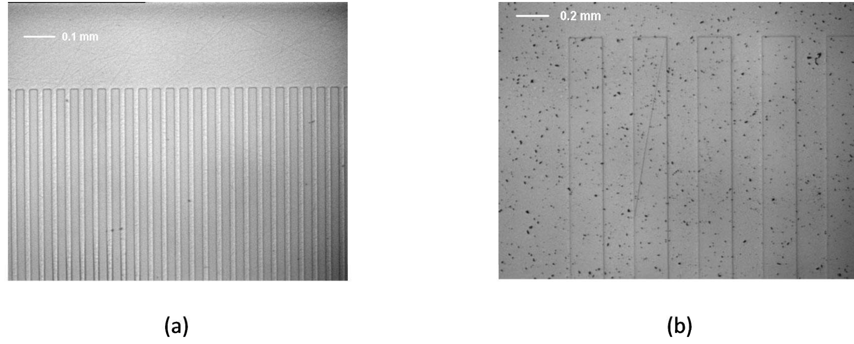

Fig. 5. Microscope images of the HF etched glass sample after periodic erasure using e-beam deposition process. (a) 42 μm period, (b) 400 μm period.

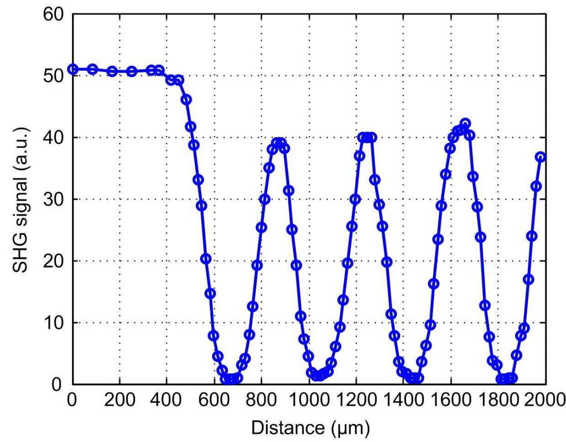

Fig. 6. SHG measurement by scanning across the 400 μm period $\chi^{(2)}$ grating fabricated by periodic erasure using e-beam deposition process.

$$\begin{pmatrix} p_x(t) \\ p_y(t) \\ p_z(t) \end{pmatrix} = \begin{pmatrix} 0 & 0 & 0 & 0 & d_{31} & 0 \\ 0 & 0 & 0 & d_{31} & 0 & 0 \\ d_{31} & d_{31} & d_{33} & 0 & 0 & 0 \end{pmatrix} \begin{pmatrix} e_x^2(t) \\ e_y^2(t) \\ e_z^2(t) \\ 2e_y(t)e_z(t) \\ 2e_x(t)e_z(t) \\ 2e_x(t)e_y(t) \end{pmatrix} \tag{2}$$

where $p_i(t)$ and $e_i(t)$ (i=x,y,z) are the time-dependent nonlinear polarization and electric fields, respectively. Therefore both TE-polarized (i.e., $e_y = e_z = 0$) and TM-polarized (i.e., $e_y = e_x = 0$) fundamental beams will produce SHG that is TM-polarized, and the corresponding nonlinear coefficients are $d_{TE} = d_{31}$ and $d_{TM} = d_{33}$.

For a waveguide QPM-SHG device of length L, the relationship between the instantaneous SHG output power, $P_{2\omega}(t)$, and the instantaneous fundamental mode input power, $P_\omega(t)$, is given by

#109008 - $15.00 USDReceived 23 Mar 2009; revised 12 May 2009; accepted 15 May 2009; published 21 May 2009
(C) 2009 OSA

$$P_{2\omega}(t)=\frac{8\pi^2 d_{eff}^2 L^2}{N_\omega^2 N_{2\omega} c\varepsilon_0 \lambda_f^2}\frac{P_\omega^2(t)}{A_{eff}}\frac{\sin^2(\Delta kL/2)}{(\Delta kL/2)^2} \tag{3}$$

where c is the vacuum speed of light, ε_0 is the permittivity of free space, λ_f is the wavelength of the fundamental mode, A_{eff} is the effective mode area, and d_{eff} is the effective nonlinearity. Expressions for the later two quantities are given by Eqs. (4) and (5)

$$A_{eff}=\frac{\left(\iint E_\omega^2(x,z)dxdz\right)^2\left(\iint E_{2\omega}^2(x,z)dxdz\right)}{\left|\iint E_\omega^2(x,z)E_{2\omega}(x,z)dxdz\right|^2} \tag{4}$$

$$d_{eff}=\frac{1}{m\pi}\frac{\left|\iint E_\omega^2(x,z)d(x,z)E_{2\omega}(x,z)dxdz\right|}{\left|\iint E_\omega^2(x,z)E_{2\omega}(x,z)dxdz\right|} \tag{5}$$

where $E_\omega(x,z)$ and $E_{2\omega}(x,z)$ are the electric field spatial distributions corresponding to the fundamental and second harmonic waveguide modes, N_ω and $N_{2\omega}$ are the effective indices of the fundamental mode and second harmonic modes, respectively, and d(x,z) is the spatial distribution of the second order nonlinear coefficient (d_{31} for the TE mode and d_{33} for the TM mode). The nonlinear coefficient relates the induced SHG polarization $p_{2\omega}$ to the fundamental electric field E_ω through the relation $p_{2\omega}(x,z)=d(x,z)E_\omega^2(x,z)$. Equations (3)-(5) follows from the results given in [28] after neglecting propagation loss and taking into account the spatial overlap between the modes and the nonlinearity. It has also been assumed that the non-linear phase matching grating has a square-wave profile with a 50:50 duty cycle. The effective area accounts for the spatial overlap between the fundamental and second harmonic modes, while the effective nonlinearity accounts for the spatial overlap between the fundamental mode, the second harmonic mode and the nonlinearity. If the nonlinearity is uniform and equal to d throughout the waveguide region, then according to Eq. (5) d_{eff} reduces to $1/m\pi$ times d.

The performance of the 1 cm long waveguide QPM-SHG device was characterized using a 1064 nm Nd:YAG MicroChip pulsed laser for the fundamental beam. The laser's pulse repetition rate (R), pulse energy and full-width-1/e pulse duration (σ_e) were of 6.5 kHz, 10.5 μJ and 0.62 ns, respectively. The fundamental beam was passed through a polarizer and variable attenuator before being coupled into the waveguide using a 20× objective lens. The output second-harmonic signal was collected by another 20× objective lens and directed to a photodiode detector after passing through an IR pump blocking filter and 532 nm narrow bandpass filter. The average SHG power vs. the average fundamental power was measured for both TE and TM-polarized fundamental beams at room temperature, and the results are shown in Fig. 7. The insert is the image of the output green light at 532 nm. Only a TM-polarized SHG signal was produced as predicted by Eq. (2). Furthermore, the average output power has quadratic dependence on the average input power as theoretically expected.

The temporal pulse shape generated by the MicroChip laser is approximately Gaussian and is given by

$$P_\omega(t)=P_\omega^{peak}\exp\left(-\frac{t^2}{2\sigma^2}\right) \tag{6}$$

with a repetition rate of R and a peak power of P_ω^{peak}, where σ is related to the full-width-1/e

#109008 - $15.00 USDReceived 23 Mar 2009; revised 12 May 2009; accepted 15 May 2009; published 21 May 2009
(C) 2009 OSA

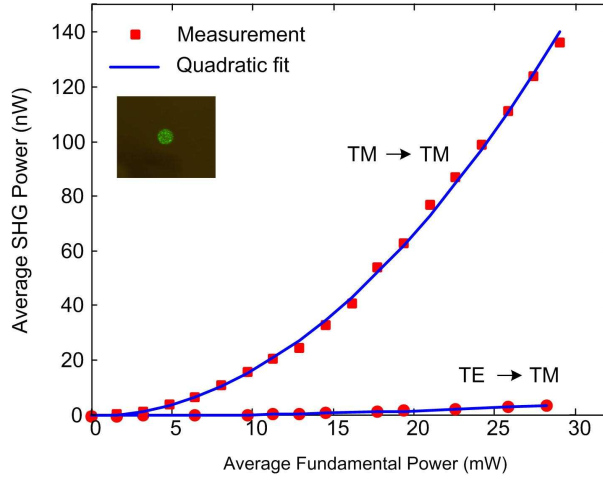

Fig. 7. Measured average SHG power vs. average fundamental power at 1064 nm for both TM and TE polarized fundamental beams.

pulse width σ_e by

$$\sigma_e = 2\sqrt{2}\sigma \tag{7}$$

Thus according to Eq. (3), the temporal pulse shape for the SHG signal will also be Gaussian and given by

$$P_{2\omega}(t) = P_{2\omega}^{peak} \exp\left(-\frac{t^2}{\sigma^2}\right) \tag{8}$$

with a repetition rate of R and a peak power of $P_{2\omega}^{peak}$. It follows from these equations that

$$\begin{aligned} P_{\omega}^{avg} &\approx R\int_{-\infty}^{\infty} P_{\omega}(t)dt = P_{\omega}^{peak}\sqrt{2\pi\sigma^2}R \\ P_{2\omega}^{avg} &\approx R\int_{-\infty}^{\infty} P_{2\omega}(t)dt = P_{2\omega}^{peak}\sqrt{\pi\sigma^2}R \end{aligned} \tag{9}$$

since $\sigma_e << 1/R$. Thus

$$\frac{P_{2\omega}^{peak}}{\left(P_{\omega}^{peak}\right)^2} = 2\sqrt{\pi}\sigma R\frac{P_{2\omega}^{avg}}{\left(P_{\omega}^{avg}\right)^2} \tag{10}$$

The conversion efficiency (in percent), η , per launched fundamental beam power per device length square can be expressed using Eqs. (3), (7) and (10) as

$$\eta = 100\frac{P_{2\omega}^{peak}(t)/P_{\omega}^{peak}(t)}{P_{\omega}^{peak}(t)/L^2} = 100\sqrt{\frac{\pi}{2}}\sigma_e R\frac{P_{2\omega}^{avg}}{\left(P_{\omega}^{avg}\right)^2 L}$$

#109008 - $15.00 USDReceived 23 Mar 2009; revised 12 May 2009; accepted 15 May 2009; published 21 May 2009
(C) 2009 OSA

$$=\frac{8\pi^2 d_{eff}^2}{N_\omega^2 N_{2\omega} c\varepsilon_0 \lambda_f^2 A_{eff}} \frac{\sin^2(\Delta kL/2)}{(\Delta kL/2)^2} \tag{11}$$

Using Eq. (11), together with the data shown in Fig. 7, the measured (at room temperature) normalized conversion efficiency for this device is found to be $9\text{x}10^{-8}$ %/W/cm^2 for a TM polarized fundamental beam.

3.2 Thermal tuning

The required phase matching period given by Eq. (1), depends critically on the dispersion of the waveguide modes, and even a small error in the computed period will result in a substantial phase mismatch. For example, a 4%, i.e. 5×10^{-4}, error in the assumed dispersion value, $N_\omega - N_{2\omega}$, will produce a phase mismatch, ΔkL, equal to 3π. The QPM SHG device was temperature tuned to determine the phase mismatch and d_{eff}. The device was mounted on a thermo-electric cooler (TEC), whose temperature could be controlled by adjusting the applied voltage. The temperature was continuously varied from 10 °C to 120 °C while the intensity of the SHG signal was monitored. The changes in the SHG output power shown in Fig. 8 are due to changes in the phase mismatch as the temperature is varied. The phase mismatch, given by Eq. (1), is repeated below

$$\Delta k(T) = \frac{2\pi N_{2\omega}(T)}{\lambda_f/2} - 2\frac{2\pi N_\omega(T)}{\lambda_f} - \frac{2\pi m}{\Lambda(T)} \tag{1}$$

where T is the temperature in absolute degrees Kelvin. Thus

$$\begin{aligned}\frac{d\Delta k(T)}{dT} &= \frac{2\pi}{\lambda_f/2}\frac{dN_{2\omega}(T)}{dT} - 2\frac{2\pi}{\lambda_f}\frac{dN_\omega(T)}{dT} + \frac{2\pi}{\Lambda^2(T)}\frac{d\Lambda(T)}{dT} \\ &\approx \frac{2\pi}{\lambda_f/2}\frac{dn_{2\omega}(T)}{dT} - 2\frac{2\pi}{\lambda_f}\frac{dn_\omega(T)}{dT} + \frac{2\pi}{\Lambda^2(T)}\frac{d\Lambda(T)}{dT}\end{aligned} \tag{12}$$

where n_ω and $n_{2\omega}$ are the refractive indices of the fused silica at the fundamental and second harmonic wavelengths. Equation (12) can be rewritten as

$$\frac{d\Delta k(T)}{dT} \approx \frac{2\pi}{\lambda_f/2}\alpha(\lambda_f/2,T) - 2\frac{2\pi}{\lambda_f}\alpha(\lambda_f,T) + \frac{2\pi}{\Lambda(T)}\beta(T) \tag{13}$$

where α and β are the thermo-optic and thermal (linear) expansion coefficients, respectively, given by

$$\alpha(\lambda,T) = \frac{dn(\lambda,T)}{dT} \tag{14}$$

$$\beta(T) = \frac{1}{\Lambda(T)}\frac{d\Lambda(T)}{dT} \tag{15}$$

The thermo-optic coefficient of fused silica is both wavelength and temperature dependent, but can be approximated by $\alpha(1064\text{ nm},\text{T}) \approx 12.1\times 10^{-6}\ {}^oK^{-1}, \alpha(532\text{ nm},\text{T}) \approx 13\times 10^{-6}\ {}^oK^{-1}$ for $273\ {}^oK < T < 400\ {}^oK$ [29]. The thermal coefficient of linear expansion of fused silica is very small and approximately equal to $0.55\times 10^{-6}\ {}^oK^{-1}$ over the same temperature range [30]. As the temperature of the sample is varied between 10 °C and 120 °C, the SHG output power goes through two relative maxima, one near a temperature of 15 °C and the other near a

#109008 - $15.00 USDReceived 23 Mar 2009; revised 12 May 2009; accepted 15 May 2009; published 21 May 2009
(C) 2009 OSA

temperature of 90 ^{o}C as shown in Fig. 8. According to Eq. (3), these maxima occur when the phase mismatch ΔkL is an odd multiple of π. The maxima at $T \approx 288\ ^{o}K$ and $T \approx 363\ ^{o}K$ corresponds to $\Delta kL = 3\pi$ and $\Delta kL = 5\pi$, respectively, since the measured ratio of the first to second maximum is approximately 3 (see Fig. 8). The predicted theoretical variation of SHG output power with temperature, assuming that the first maxima occurs at $\Delta kL = 3\pi$, has been computed using Eq. (13), and the result is also shown in Fig. 8. The deviations between the theoretical and experimental data cannot be completely explained, but may be due to imperfect mode matching along the length of the QPM grating.

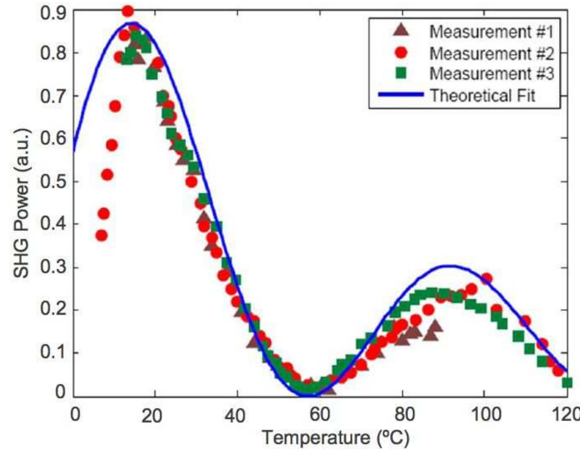

Fig. 8. Thermal tuning of the phase matching condition in the waveguide QPM-SHG device in bulk fused silica.

Assuming that the first peak in Fig. 8 corresponds to $\Delta kL = 3\pi$ and that the coupling efficiency into the device is around 30% (a reasonable estimate), the conversion efficiency with respect to launched power at $\Delta kL = 0$ would be approximately 2×10^{-5} %W^{-1}cm^{-2}. Using the waveguide mode profiles shown in Fig. 3, the effective mode area, A_{eff}, was calculated from Eq. (4) to be 86 μm^2. Combining this value with the normalized conversion efficiency of 2×10^{-5} %W^{-1}cm^{-2}, we can infer a d_{eff} of 0.0075 pm/V. This d_{eff} values is approximately 30 times smaller than expected for a uniformly poled sample with a d of 0.25 pm/V [19]. It has been recently reported that the thermally-induced nonlinearity may be reduced in femtosecond-laser-modified fused silica [31]. Similar effects have been seen in thermally-poled UV-written waveguides [32]. The opposite effect, however, was previously reported [33], and a relatively efficient electro-optic modulator has been demonstrated in thermally poled, femtosecond, laser-written waveguides [19]. Thus the conditions for which the nonlinearity is either reduced or enhanced due femtosecond-laser material modification remain unknown.

There are several possible explanations, outlined below, for the low d_{eff} reported in this paper. The most likely candidates are: (1) the peak of the thermally-induced nonlinearity is not located in the waveguide region, (2) the modulation depth of the nonlinear QPM grating is reduced by the x-ray/electron beam erasure process, (3) the duty cycle of the fine period QPM nonlinear grating is much less than 50% in the waveguide region [7] and/or (4) the femtosecond waveguide writing process greatly reduces the effectiveness of thermal poling in the waveguide region. The fourth possibility is not likely, since an efficient electro-optic waveguide modulator was demonstrated using a similar technique [19]. It should be possible to greatly improve the conversion efficiency by reducing the effective area of the modes and optimizing the QPM grating structure.

#109008 - $15.00 USDReceived 23 Mar 2009; revised 12 May 2009; accepted 15 May 2009; published 21 May 2009
(C) 2009 OSA

4. Conclusion

In conclusion, we have successfully demonstrated the combination of glass thermal poling with femtosecond laser direct writing technologies to realize a waveguide QPM-SHG device in bulk fused silica. We developed a novel method to fabricate the QPM $\chi^{(2)}$ gratings by using a standard e-beam evaporator deposition system together with a silicon grating mask to perform selective erasure of the nonlinearity in a uniformly poled region. Although the physical origin of the erasure is still not fully understood, we suspect that x-rays produced by Bremsstrahlung in the deposition chamber play an important role. We achieved normalized conversion efficiency of 2×10^{-5} %/W/cm^2 in a 1 cm long waveguide QPM device, corresponding to an effective nonlinear coefficient, 0.0075 pm/V. It should be possible to greatly improve the conversion efficiency by reducing the effective area of the modes and optimizing the QPM grating structure.

#109008 - $15.00 USDReceived 23 Mar 2009; revised 12 May 2009; accepted 15 May 2009; published 21 May 2009
(C) 2009 OSA